Pharm Res (2013) 30:655–669
DOI 10.1007/s11095-012-0894-2

RESEARCH PAPER

Pharmacokinetic and Pharmacodynamic Modeling of Romiplostim in Animals

Wojciech Krzyzanski • Liviawati Sutjandra • Juan Jose Perez-Ruixo • Bethlyn Sloey • Andrew T. Chow • Yow-Ming Wang

Received: 21 June 2012 / Accepted: 24 September 2012 / Published online: 19 December 2012

ABSTRACT

Purpose Romiplostim is a novel thrombopoiesis-stimulating peptibody that targets the thrombopoietin c-Mpl receptor, resulting in increased platelet production. The pharmacodynamic-mediated disposition (PDMDD) and its stimulatory effect on platelet production in Sprague-Dawley rats, rhesus monkeys, and cynomolgus monkeys following IV bolus and SC administration at various dose levels were determined.

Methods The pharmacokinetic (PK) profile was described by a PDMDD model that accounts for romiplostim binding to the c-Mpl receptor. The PD model contained a series of aging compartments for precursor cells in bone marrow and platelets. The stimulatory function was described by an on-and-off function operating on the fractional receptor occupancy (RO). The threshold effect, RO_{thr}, and K_D parameters were determinants of drug potency, whereas S_{max} reflected drug efficacy.

Results The model implicated that receptor-mediated clearance was negligible. RO_{thr} estimated occupancies were 0.288, 0.385, 0.771 for rats, rhesus, and cynomolgus monkeys, respectively. The analogous estimated values of K_D were 4.05, 2320, and 429 ng/mL, implying that romiplostim was much more potent in rats, which was confirmed by a dose-response (ratio of peak platelet count to baseline) relationship.

Conclusions The model adequately described romiplostim serum concentrations and platelet counts in rats, rhesus monkeys, and cynomolgus monkeys, and quantified linear clearance, PDMDD, and potency of romiplostim.

KEY WORDS c-Mpl receptor · peptibody · pharmacodynamics-mediated drug disposition (PDMDD) · pharmacokinetic and pharmacodynamic modeling

ABBREVIATIONS

$AUC_{0-\infty}$	area under the curve from 0 to infinity
BaF3-Mpl cells	Mpl-transfected cells
CFU	colony-forming unit
CL	clearance
CV	coefficient of variation
D_{IV}	intravenous dosing
ELISA	enzyme-linked immunosorbent assay
eTPO	endogenous TPO
IgG1	human immunoglobulin G subtype 1
ITS	iterative-two-stage
rHu-TPO	recombinant human thrombopoietin
TPO	thrombopoietin

INTRODUCTION

Megakaryocytopoiesis is a continuous developmental process of platelet production regulated by a complex

W. Krzyzanski
Department of Pharmaceutical Sciences, University at Buffalo
Buffalo, New York, USA

L. Sutjandra · J. J. Perez-Ruixo · B. Sloey · A. T. Chow
Amgen Inc., Pharmacokinetics and Drug Metabolism
Thousand Oaks, California, USA

Y.-M. Wang
Office of Clinical Pharmacology, Food and Drug Administration
Washington, District of Columbia, USA

J. J. Perez-Ruixo (✉)
Quantitative Pharmacology
Pharmacokinetics and Drug Metabolism Department, Amgen Inc.
Picayo 3, Puzol 46530 Valencia, Spain
e-mail: juanjose@amgen.com

network of hematopoietic growth factors. In this process, hematopoietic stem cells undergo proliferation, differentiation, and maturation, generating megakaryocytes and platelets. Platelet production is controlled by signaling through the hematopoietic c-Mpl receptor (1). The ligand for this receptor is thrombopoietin (TPO), a hematopoietic growth factor produced in the liver and marrow stroma, which is the primary regulator of megakaryocyte development and subsequent platelet formation (2). Upon binding to c-Mpl receptor, TPO triggers several cellular signal transduction processes, which involve the JAK-STAT and tyrosine kinase pathways, the mitogen-activated protein kinase pathway, the phosphatidylinositol 3-kinase pathway, and the nuclear factor kappa B pathway (3,4). Early recombinant forms of TPO showed promising clinical results when administered in human. However, later studies failed to meet the clinical endpoints, because the recombinant proteins generated antibodies that cross-reacted with c-Mpl ligands and resulted in paradoxical thrombocytopenia (5,6). Further clinical development of most of these molecules was therefore suspended (7).

Romiplostim (Nplate®, previously known as AMG 531) is a novel biological TPO stimulating agent developed to overcome the problem of cross-reacting antibodies by use of a random peptide sequence to activate the c-Mpl receptor. Structurally, romiplostim is a 59 kD fusion protein that consists of c-Mpl binding domain covalently linked to the N-terminus of the carrier Fc domain (8). The c-Mpl receptor binding domain contains two peptide chains each with two units of a novel TPO mimetic peptide. The four copies of the TPO mimetic peptide stimulate megakaryocytopoiesis in the same ways as TPO, and bear no sequence homology with TPO, thus further reducing the potential for the generation of anti-TPO antibodies. *In vitro*, romiplostim competes with TPO for the binding to c-Mpl receptor on normal platelets and Mpl-transfected cells (BaF3-Mpl cells). Upon binding to the c-Mpl receptor, romiplostim activates JAK-STAT and other pathways similarly to TPO (3). When co-cultured with the murine bone marrow cells, romiplostim promotes the growth of CFU-megakaryocytes and promotes the proliferation as well as the maturation of megakaryocytes (3). During preclinical development romiplostim evidenced robust platelet responses in mice, rats, rabbits and monkeys (data on file). Currently, romiplostim has been approved in the USA, EU and other countries for the treatment of patients with immune thrombocytopenia (9).

Similarly to TPO (10), romiplostim binds to the c-Mpl receptor (11) and exhibits target-mediated drug disposition (TMDD), which occurs when the time course of the drug concentration is influenced by the interaction between the drug and its pharmacological target (12). General pharmacokinetic models have been developed to account for drug-receptor binding, internalization and degradation, as well as the receptor turnover (13,14). These models are particularly useful in analysis of hematopoietic growth factors and newly emerging targeted therapies that are highly specific, very potent and effective at much lower drug concentrations than small molecule agents. TMDD models have been applied to describe pharmacokinetics of hematopoietic growth factors, such as erythropoietin (15), pegfilgrastim (16), and TPO-stimulating agents (17–19), and other biological drugs such as monoclonal antibodies (20–22) and cytokines (23,24). Clearance of these receptor-mediated compounds saturates at higher concentrations originating non-linear pharmacokinetics, which is dependent on free receptor expression. At the same time, free receptor expression is determined by the receptor turnover in individual cells and the turnover of cells expressing the target receptor. Because romiplostim induces an increase of the number of megakaryocytes and platelets that carry receptors capable of clearing romiplostim and TPO, a self-regulating cycle is formed, which leads to a strong interaction between the non-linear pharmacokinetics and the pharmacodynamics of romiplostim. This phenomenon known as pharmacodynamic-mediated drug disposition (PDMDD) has been recently described for romiplostim in healthy subjects (19).

The objective of this study was to determine the pharmacokinetics and the stimulatory effect of romiplostim on platelet production in rats, rhesus monkeys, and cynomolgus monkeys. We applied combinations of previously published PK/PD models describing receptor-mediated drug disposition (14,19,25) and stimulation of platelet production (26) to quantify the PDMDD of romiplostim in these animal species.

MATERIALS AND METHODS

Study Drug

Romiplostim and vehicle were manufactured by Amgen Inc. (Thousand Oaks, CA). Dosing solutions were prepared by diluting the romiplostim with vehicle at appropriate concentrations and volumes to achieve the intended doses.

Animal Experiments

All procedures used in the studies adhered to the Principles of Laboratory Animal Care. Animals were treated humanely in accordance with the USDA Animal Welfare Act (9 CFR, Parts 1, 2, and 3) and the conditions specified in the Guide for Care and Use of Laboratory Animals (ILAR publication, 1996, National Academy Press). Sprague-Dawley rats, rhesus

monkeys and cynomolgus monkeys were used in the experiments. Animals were maintained under laboratory standard conditions on a 12 h light/dark cycle, and in a temperature- and humidity-controlled room. Animals received Harlan Teklad Certified Rodent or Primate Diet and *ad libitum* access to water. The same formulation was used for IV and SC dosing in all the studies described below.

Rat Study

Twenty-four male Sprague-Dawley rats (250 to 350 g) were divided into six groups and received a single intravenous (IV) bolus or subcutaneous (SC) dose of romiplostim at 0.03, 0.1 or 0.3 mg/kg. To evaluate the pharmacokinetics, an alternative sparse sampling schema design was selected. Approximately 0.35 mL of whole blood was collected from a jugular cannula or a tail vein at predose, 5 and 20 min, 2, 8, 16, 30, 42, 56, and 96 hours postdose from two animals in each dose group. From two other animals, whole blood was collected at predose, 10 min, 1, 4, 12, 24, 36, 48, 72, and 120 h postdose. To determine the platelet count, approximately 0.15 mL of whole blood was collected at predose and then daily up to 21 days postdose from 4 rats in each group.

Rhesus Monkey Study

Eighteen male rhesus monkeys (3.0 to 3.7 kg) were divided into six groups and received a single IV bolus or SC dose of romiplostim of 0.5, 2.0 or 5.0 mg/kg. Whole blood samples (approximately 0.75 mL) were collected for PK analyses via venipuncture at predose, 5, 15, and 30 min, 1, 2 ,4, 8, 12, 24, 48, 72, 120, 168, 240, 288, 312, 336, 360, 408, 456, and 504 h postdose in all dose groups. In addition, blood was collected at 192 (0.5-mg/kg and 5.0-mg/kg dose groups only) hours postdose; 216 and 264 (0.5-mg/kg and 2.0-mg/kg dose groups only) hours postdose; 552 (2.0-mg/kg dose groups only) hours postdose; and at 576 and 648 (5.0 mg/kg dose groups only) hours postdose. To determine the platelet count, approximately 0.5 mL of whole blood was collected at predose, 3, 5, 7, 10, 12, 13, 14, 15, 17, 19, and 21 days postdose in all six groups. Additional sampling was performed at 8, 9, and 11 days postdose in the 0.5-mg/kg dose groups; at 23 days postdose in the 2.0-mg/kg dose groups; and at 24 and 27 days postdose in the 5.0-mg/kg dose groups.

Cynomolgus Monkey Study

Nine male cynomolgus monkeys (2.7 to 3.6 kg) were divided into three groups and received a romiplostim single IV bolus of 0.5 or 5.0 mg/kg or SC dose of 5.0 mg/kg. Whole blood samples (approximately 0.75 mL) were collected for PK analyses via venipuncture at predose, 5, 15, and 30 min, and at 1, 2, 4, 8, 12, 24, 48, 72, 120, 168, 216, 264, 312, 360, 408, 456, and 504 h postdose. In addition, approximately 0.5 mL of whole blood samples were collected for platelet count determination at predose, 3, 5, 7, 8, 9, 10, 11, 12, 13, 14, 15, 17, 19, 21, 24, 27, and 30 days postdose.

Bioanalytical Methods

Serum concentrations of romiplostim were determined by use of a modified colorimetric enzyme-linked immunosorbent assay (ELISA) as previously described (7). The lower limit of quantification was 18 pg/mL and the total coefficient of variation (CV) ranged from 7 to 17% across the validated range of concentration, which extended up to 500 pg/mL. Platelet counts were determined using routine hematology laboratory methods.

Noncompartmental Analysis

To evaluate the nonlinearity in romiplostim pharmacokinetics, the C_{max}, $AUC_{0\text{-}\infty}$, and CL parameters were calculated for each animal using the noncompartmental approach implemented in WinNonlin (Pharsight Corporation, Mountain View, CA). The nonlinearity was evaluated by proportionality of these parameters with IV dose. To determine if the nonlinearity was related to receptor binding, a relationship between volume of distribution (V) and IV dose was also examined (14). Due to the sparse sampling design in rat studies, the non-compartmental parameters for rats were calculated based on the composite mean concentration–time data; whereas for the other animal species, they were calculated for individual animals because serial PK samples were collected from each animal.

Pharmacokinetic Model

Romiplostim is a fusion protein with TPO mimetic peptides that have similar binding affinity to c-Mpl receptor as TPO. Therefore, a target-mediated disposition model was considered to analyze romiplostim pharmacokinetics. Consequently, an open two-compartment model with the receptor mediated binding, non-specific distribution to extravascular tissues (Q), and first-order (CL) elimination pathway was selected (Fig. 1). The internalization process was initially considered and eventually neglected due to consistently small estimates of the internalization rate constant k_{int} for all animal species, possibly due to the romiplostim high molecular weight and steric hindrance. To avoid estimation of the binding (k_{on}) and dissociation (k_{off}) constants, the quasi-equilibrium between romiplostim free concentration and c-Mpl receptors was assumed as previously described (14,25). Four c-Mpl receptor molecules can potentially bind to one molecule of romiplostim. However, because c-Mpl is a membrane

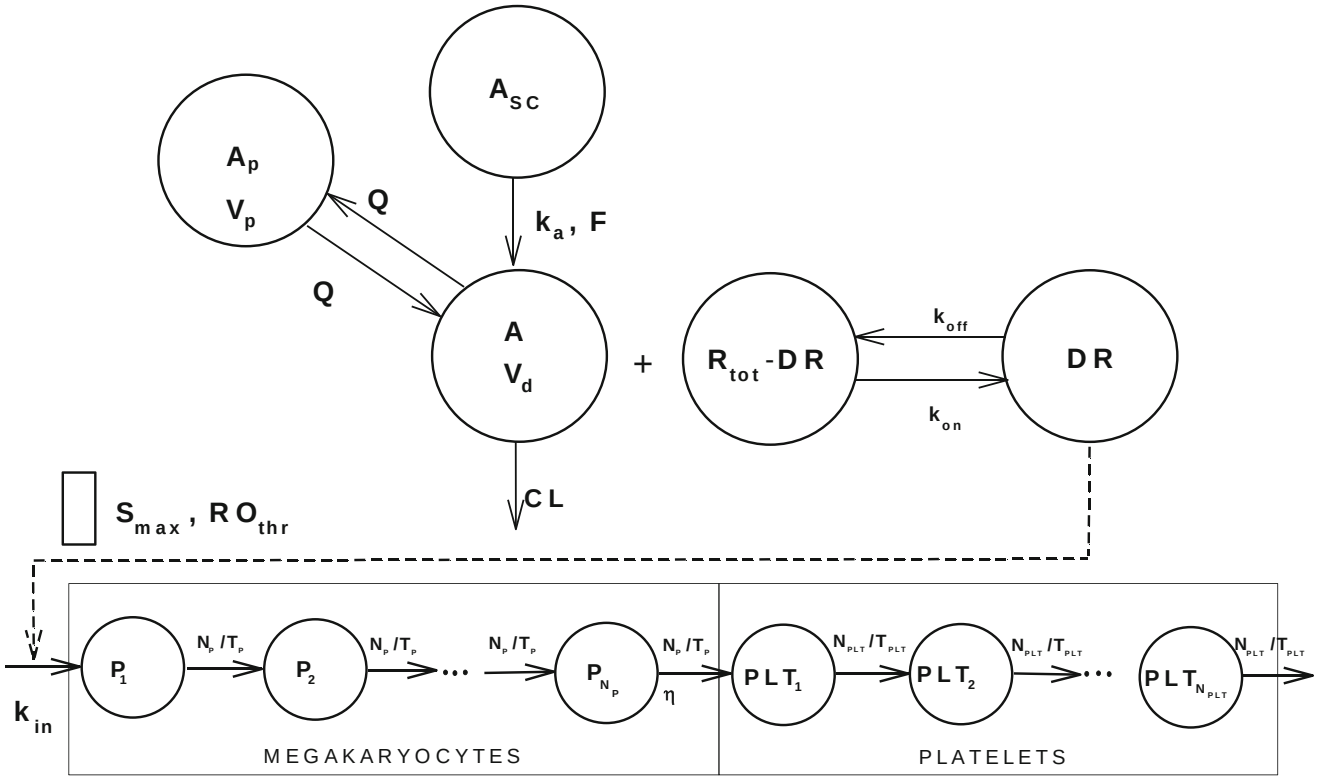

Fig. 1 Schematic diagram of a PK/PD model of romiplostim's effects on platelet counts in rats and monkeys that accounts for c-Mpl receptor binding. Symbols, processes, and model operation are explained in "Materials and Methods".

receptor and the romiplostim concentration is generally in excess relative to c-Mpl in the body, the stoichiometry binding was assumed to be 1:1. In addition, the SC absorption of romiplostim was represented by the first-order absorption rate, k_a. Absolute bioavailability (F) was estimated by simultaneously analyzing the data obtained after IV and SC administration. Therefore, the differential equations describing the pharmacokinetics of romiplostim were as follows:

$$\frac{dA_{SC}}{dt} = -F \cdot k_a \cdot A_{SC} \tag{1}$$

$$\frac{dC_{tot}}{dt} = \frac{F \cdot k_a \cdot A_{SC}}{V_d} - \frac{(CL + Q) \cdot C}{V_d} + \frac{Q \cdot C_p}{V_d} \tag{2}$$

$$\frac{dC_p}{dt} = \frac{Q}{V_p} \cdot (C - C_p) \tag{3}$$

where, A_{SC} was the amount of romiplostim in the absorption site; V and V_p were the volumes of the central and peripheral compartments, respectively; C was unbound romiplostim serum concentration; C_{tot} was the total romiplostim serum concentration; and C_p was the unbound romiplostim concentration in peripheral compartment. The unbound romiplostim serum concentration was calculated from the equilibrium Equation (25):

$$C = \frac{1}{2}\left[C_{tot} - R_{tot} - K_D + \sqrt{(C_{tot} - R_{tot} - K_D)^2 + 4 \cdot K_D \cdot C_{tot}}\right] \tag{4}$$

The total c-Mpl receptor density (R_{tot}) was assumed to be proportional to the platelet and megakaryocyte counts and was described by the following equation (19):

$$R_{tot} = \xi \cdot (PLT + \eta \cdot MK) \tag{5}$$

where ξ represents the number of c-Mpl receptors per cell. Here PLT denotes platelet counts in blood and MK megakaryocytes counts in bone marrow. The factor η=4000 denotes the conversion factor equal to the average number of platelets shed by a megakaryocyte during thrombopoiesis. The variables PLT and MK are described below in the PD model. The absolute receptor occupancy, DR, was calculated as follows:

$$DR = \frac{R_{tot} \cdot C}{K_D + C} \tag{6}$$

where the dissociation equilibrium constant is denoted as K_D.

Pharmacodynamic Model

Megakaryocytopoiesis is mostly regulated by endogenous thrombopoietin (eTPO) that stimulates proliferation and maturation of platelet progenitors, which included high proliferative-potential megakaryocytes, burst-forming-unit megakaryocytes, colony-forming-unit megakaryocytes, promegakaryoblasts, megakaryoblasts and mature megakaryocytes. Each mature megakaryocyte releases several thousand platelets to the circulation. Circulating platelets are removed from the blood by various mechanisms involving random destruction and programmed cell death. c-Mpl receptors are expressed on megakaryocyte progenitors, megakaryocytes, and platelets. Binding to c-Mpl receptors followed by degradation is considered a major machenism for clearance of eTPO (10). Although romiplostim competes with eTPO for the same c-Mpl receptors and exerts the same pharmacological effect, eTPO concentrations were not incorporated into the PK-PD model because they were not consistently measured experimentally and were relatively low compared to the romiplostim serum concentrations achieved after drug administration and, consequently, the amount of eTPO bound to c-Mpl receptor is negligible relative to the amount of romiplostim bound to that receptor, particularly in the animal experiments described herein, in which thrombocytopenia was not present. The model assumes that after binding to the c-Mpl receptor, romiplostim generates a stimulus (messenger), which is proportional to the fraction of receptors occupied by the drug (equation 7).

$$S = e \cdot \frac{DR}{R_{tot}} = \frac{e \cdot C}{K_D + C} \tag{7}$$

where e is the proportionality factor denoting the power of the romiplostim to produce the stimulus. Furthermore, the stimulus activates the production rate of megakaryocyte precursors according to a step function represented by an on-and-off function:

$$H(S) = \begin{cases} S_{\max}, & if\ S > S_{thr} \\ 0, & if\ S \le S_{thr} \end{cases} \tag{8}$$

where S_{max} is the maximal stimulus, and S_{thr} denotes the threshold stimulus triggering the maximal stimulus. According to equation 7, S_{thr} equals the product $e \cdot RO_{thr}$, where RO_{thr} is the threshold receptor occupancy triggering S_{max}. The model assumed that the production rate of megakaryocyte precursors was a zero-order process quantified by k_{in}. Therefore, the differential equation describing the effect of romiplostim on the production rate of megakaryocyte precursors, P_1, was as follows (equation 9):

$$\frac{dP_1}{dt} = k_{in} \cdot (1 + H(S)) - \frac{N_P}{T_P} \cdot P_1 \tag{9}$$

The pharmacodynamic model depicted in Fig. 1 applied the concept of a maturation-structured cytokinetic model previously introduced (26), which detailed the development and maturation of platelet precursors in the bone marrow and platelets in blood. The same concept has been exploited further to deal with the dynamics of neutrophils and red blood cells following the administration of pegfilgrastim and erythropoietin, respectively (16,27). Briefly, the precursors were represented by a series of aging compartments (N_P=10) with the first-order transition rates N_P/T_P, where T_P denotes the mean life span of precursor cells in bone marrow.

$$\frac{dP_i}{dt} = \frac{N_P}{T_P} \cdot (P_{i-1} - P_i), \qquad i = 2, \ldots, N_P \tag{10}$$

Similarly, platelets are represented by a series of sequential aging compartments (N_{PLT}=10) with the transition rates N_{PLT}/T_{PLT}, where T_{PLT} is the mean lifespan of a circulating platelet.

$$\frac{dPLT_1}{dt} = \frac{\eta N_p}{T_p} \cdot P_{N_P} - \frac{N_{PLT}}{T_{PLT}} \cdot PLT_1 \tag{11}$$

$$\frac{dPLT_j}{dt} = \frac{N_{PLT}}{T_{PLT}} \cdot \left(PLT_{j-1} - PLT_j\right), j = 2, \ldots, N_{PLT} \tag{12}$$

The platelet count (PLT) was the sum of platelet counts in each of aging compartment

$$PLT = PLT_1 + \ldots + PLT_{NPLT} \tag{13}$$

and the megakaryocyte count was represented as the sum of precursor cells in each aging compartment

$$MK = P_1 + \ldots + P_{NP} \tag{14}$$

The number of 10 compartments was arbitrarily selected in order to have a large enough number of compartments that result in a smoothed distribution of cell lifespan by reducing the variability in the cellular transit time (28). In addition, it is assumed that the only loss of cells in the sequential aging compartments is into the next compartment. Consequently, the random loss of both precursor and platelets was assumed to be negligible in order to avoid identifiability problems and, therefore, the estimated lifespan of precursor and platelets becomes apparent. Baseline (steady-state) values were used as the initial conditions as follows:

$$P_i(0) = \frac{T_P}{\eta N_P T_{PLT}} PLT_0, \qquad i = 1, \ldots, N_P \tag{15}$$

$$PLT_j(0) = \frac{PLT_0}{N_{PLT}}, \qquad j = 1, \ldots N_{PLT} \tag{16}$$

The baseline platelet count, PLT_0, was used to calculate k_{in} as a secondary parameter according to equation 17:

$$k_{in} = \frac{PLT_0}{\eta T_{PLT}} \tag{17}$$

Statistical Analysis

A non-linear mixed effects analysis was performed for each animal species independently and a simultaneous analysis of PK and PD data within each animal species (19) was conducted in NONMEM® Version 7.2.0 (Icon Development Solutions, Ellicott City, MD, USA) with a GFortran 4.5 compiler. The ADVAN13 subroutine and the first-order conditional estimation method with interaction (FOCEI) were used for the key intermediate model analysis. The stochastic approximation expectation maximization (SAEM) method was used to provide the parameter estimation of the final model (29). After 1000 iterations, the objective function value (OFV) and standard error were obtained by running the iterative-two-stage (ITS) method with the final parameter estimates. Graphical data visualization, evaluation of NONMEM® outputs, construction of goodness-of-fit plots and graphical model comparisons were conducted using TIBCO Spotfire S +Version 8.2.0 (TIBCO Software Inc., Palo Alto, CA, USA). The between animal variability of selected PKPD parameters was described by the exponential model:

$$P = \theta_P \cdot \exp(\eta_P) \tag{18}$$

where P is the individual parameter value, θ_P is its population geometric mean (or typical value), and η_P is an independent random variable normally distributed with zero mean and standard deviation ω_P. The exponential model of the residual error was also applied to both drug serum concentration and platelet count data:

$$Y = \hat{Y} \cdot \exp(\varepsilon) \tag{19}$$

where Y is the observation, $\hat{Y}$ is the corresponding model prediction and ε is assumed to be an independent and normally distributed random variable with the zero mean and standards deviation σ. Model performance was evaluated by means of the visual predictive check (30).

Model-Based Simulations

A series of simulations were performed to compare the differences in PK and PD romiplostim time profiles between three animal species. The fractional receptor occupancy was plotted as a function of romiplostim serum concentrations. Additionally, the PLT profiles were simulated for an array of doses and the peak values, PLT_{max}, were determined. The ratio PLT_{max}/PLT_0 was plotted against doses to obtain dose-response relationship for each species. The typical model parameter values were used for simulations.

RESULTS

The results of noncompartmental analysis are shown in Table I. The ratios C_{max}/D_{IV} and CL did not differ between dose groups for rats and monkeys, implicating linear clearance of romiplostim for those species. On the other hand, V_{ss} ($V+V_p$) decreases with increasing D_{IV} for rats and monkeys. This pattern is consistent with a target-mediated disposition where the drug-receptor complex internalization rate is negligible (14) and implies that the estimates of the k_{int} would be small. This was confirmed by fitting the naïve pooled data for each species with the PK/PD model, which resulted in k_{int} estimates close to 0. Subsequently, the internalization process was not included in the PKPD model.

The rat, rhesus, and cynomolgous monkeys PKPD data were fitted to the semi-mechanistic model that incorporates the c-Mpl receptor-mediated disposition. The model parameter estimates are presented in Table II. The observed PK and PD profiles for individual animals together with the corresponding model predictions are displayed in Figs. 2, 3 and 4.

Rat Model

The PK model adequately described the romiplostim serum concentrations observed in individual rats after IV and SC administration (Fig. 2a and b). The observed romiplostim serum concentrations show a bi-exponential pattern. The mean V and CL of romiplostim was 0.0550 L/kg and 8.09 mL/h/kg, respectively. The V_p was estimated to be 0.0622 L/kg. The estimate K_D, reported in mass/volume units and then converted to molar units using the romiplostim molecular weight of 59 kD, was 68 pM. A conversion factor of ξ=0.0682 fg/cells resulted in an estimate of 696 c-Mpl molecules per platelet. This number is comparable to the reported value of 233 receptors per cell (31).

In rats, the observed mean platelet data exhibited a lag time of 48 h, after which the platelet responses increased to reach the peak values of 2370, 3530, and $3520 \cdot 10^6$cells/mL for IV doses of 30, 100, and 300 μg/kg, respectively. The peak times also increased with doses and were 7, 9, and 10 days, respectively. Notably, a similar time course of platelet counts was observed after SC administration of the same dose levels, except for the platelet peak following the SC 100-mg/kg dose, which was higher to the peak obtained following the SC 300-mg/kg dose. The individual time courses of platelet counts were well described by the model. The T_P estimate is consistent with its interpretation as a

Table I Summary of Mean (SD) Non-compartmental Pharmacokinetic Parameters Following a Single IV or SC Dose of Romiplostim in Rats, Rhesus Monkeys, and Cynomolgus Monkeys

Species	Dose (mg/kg)	Route	Parameter					
			C_{max} (ng/mL)	T_{max} (h)	$AUC_{0-\infty}$ (h·ng/mL)	CL or CL/F (mL/hr/kg)	V (mL/kg)	V_{ss} (mL/kg)
Rats	0.03	IV	687	0	2850	7.72	32	139
	0.1	IV	2680	0	12500	6.33	29.5	118
	0.3	IV	7240	0	35600	8.44	41.4	114
	0.03	SC	18.9	16	793	27.7	NA	NA
	0.1	SC	83.5	8	3350	23.5	NA	NA
	0.3	SC	234	12	7310	41.0	NA	NA
Rhesus Monkeys	0.5	IV	8970 (790)	0	67200 (1920)	7.44 (0.22)	NA	196 (17.4)
	2.0	IV	34100 (3530)	0	283000 (90300)	7.63 (2.69)	NA	184 (35.4)
	5.0	IV	117000 (48200)	0	660000 (11900)	7.76 (1.55)	NA	184 (4.01)
	0.5	SC	1450 (219)	8	49500 (4820)	10.2 (1.05)	NA	NA
	2.0	SC	4080 (1670)	8	135000 (57000)	17.0 (7.80)	NA	NA
	5.0	SC	14900 (6550)	4	294000 (44400)	17.3 (2.85)	NA	NA
Cynomolgus Monkeys	0.5	IV	6580 (173)	0	25600 (5390)	20.1 (4.13)	76 (2.02)	198 (20.7)
	5.0	IV	88100 (24700)	0	291000 (30100)	17.3 (1.82)	60.2 (18.8)	110 (21.1)
	5.0	SC	3020 (1880)	4	56000 (20500)	99.2 (41.2)	NA	NA

NA not available

precursor maturation time. Similarly, the T_{PLT} estimate is consistent with the platelet lifespan in rats (32). The maximal increase in the production rate for platelet precursors due to romiplostim stimulation is about 2.91-fold in rats and the threshold receptor occupancy that triggers the stimulus, RO_{thr}, indicates that almost 29% receptors need to be activated by romiplostim in order to elicit pharmacological effect. Between animal variability in model parameters was relatively low, except for the S_{max}.

Rhesus Monkey Model

Following an IV bolus dose, the PK profiles rapidly descended to a slower phase that started for all doses at about 24 h. The slower decline for romiplostim serum concentrations ended in a yet slower phase at a different time depending on the dose. The terminal slopes of the romiplostim serum concentration were also dose-dependent. Interestingly, the post-absorption phases of the romiplostim PK profiles after SC administration were similar to those observed following IV dosing. The estimates of V and CL (normalized by body weight) were very similar to those estimated for rat. The estimate of bioavailability F was at the boundary and was subsequently fixed at 1. The k_a was higher for rhesus monkeys compared to rats (Table II). The estimate of K_D, 39.3 nM, was 573-fold higher than the value estimated for rats. The estimate of the number of c-Mpl receptor per platelet was $1.39 \cdot 10^5$.

As it was observed in rats, the mean platelet responses following IV dosing in rhesus monkeys exhibited a lag time of 72 h followed by a rapid increase to a peak value of 680, 857, and $1260 \cdot 10^6$ cells/mL for increasing doses, respectively. However, the pre-dose mean platelet counts differed between dose groups: 450, 417, and $516 \cdot 10^6$ cells/mL for the 0.5-, 2-, and 5-mg/kg doses, respectively. The peak for the lowest dose mean platelet data occurred at the latest time of 216 h owing to a flat peak region. The remaining peak times were 168 and 192 h for the 2- and 5-mg/kg doses, respectively. Notably, the observed time course of platelet count following IV dosing was similar to that observed after SC administration of the same dose level. The model predicted platelet responses well, except for the middle SC dose where the median predictions were slightly larger than the observations. The T_P and T_{PLT} estimates for rhesus monkeys were 4.6 days and 7.6 days, respectively. The T_P estimate reflects the average lag time before the individual platelet counts start to increase. The S_{max} and RO_{thr} estimates were 9.31 and 0.385, respectively. This implies that the maximal increase in the production rate for platelet precursors due to romiplostim stimulation is about 9.3-fold. Between animal variability in model parameters was relatively low, except for the S_{max} and k_a.

Cynomolgus Monkey Model

Similar to what was observed in rhesus monkeys, the time course of romiplostim concentration initially declined to reach a slower decay rate at 24 h. This phase lasted up to

Table II The Estimates of the Fixed and Random Effects Parameters Together with Their Relative Standard Errors

Parameters	Units	Rat Typical Value (RSE)	Interindividual~% CV (RSE)	Rhesus Typical Value (RSE)	Interindividual~%CV (RSE)	Cynomolgus Typical Value (RSE)	Interindividual~% CV (RSE)
CL	L/h/kg	0.00809 (5.64)	9.61 (55.8)	0.00726 (23.0)	23.0 (38.4)	0.0197 (131)	14.9 (50.2)
V	L/kg	0.0550 (8.96)	10.4 (90.5)	0.051 (23.5)	20.0 (50.0)	0.0709 (506)	60.6 (31.1)
Q	L/h/kg	0.00484 (22.1)		0.000194 (17.3)		0.000912[b]	
V_p	L/kg	0.0622 (13.1)		0.0517 (14.9)		0.336[b]	
k_a	h^{-1}	0.0686 (15.0)	15.3 (4.94)	0.118 (29.9)	66.6 (49.5)	0.0374[b]	
F		0.304 (20.8)	26.3 (72.9)	1[a]		0.375[b]	
K_D	ng/mL	4.05 (12.9)		2320 (29.0)		429[b]	
ξ	fg/cell	0.0682 (15.8)		13.6 (40.6)	27.3 (50.9)	1.33[b]	
T_P	h	47.8 (6.36)		111 (7.52)		114 (255)	
T_{PLT}	h	148 (8.38)	18.9 (8.6)	183 (13.2)	12.8 (31.2)	171 (119)	24.2 (67.3)
PLT_0	10^9 cells/L	869 (9.60)	17.4 (3.00)	392 (15.4)	11.7 (28)	441 (125)	18.4 (72.9)
S_{max}		2.91 (24.1)	45.2 (1.95)	9.31 (77.3)	54.0 (28.8)	18.9 (338)	35.5 (62.5)
RO_{thr}		0.288 (9.72)		0.385 (17.4)		0.771[b]	
$\eta_{TPLT\text{-}PLT0}$		−0.0157 (5.93)		0.00399 (67.9)			
$\eta_{TPLT\text{-}Smax}$		0.0642 (3.01)		0.0368 (38.3)			
$\eta_{PLT0\text{-}Smax}$		−0.0660 (1.47)		−0.014 (89.3)			
Residual variability (%CV)							
σ_C^2		15.8 (629)		35.2 (284)		39.0 (257)	
σ_{PLT}^2		11.4 (876)		13.0 (769)		17.0 (588)	

[a] parameter was fixed

[b] RSEs were not obtained

216 h, when the terminal phase with a much smaller slope started. The model adequately described the observed individual romiplostim serum concentrations. The mean estimate of V was similar and CL was 2.7-fold higher than the corresponding (body weight normalized) estimate values for rhesus monkeys. The Q and V_p was 4.7- and 6.5-fold larger than the corresponding parameter obtained in rhesus monkeys. The k_a was lowest of the studied species. The estimate of K_D, 7.27 nM, was approximately 18.5% of the value for rhesus monkeys. The estimate of the number of c-Mpl receptor per platelet was $1.36 \cdot 10^4$.

The mean platelet count after a lag time of about 48 h climbed to a peak value $686 \cdot 10^6$ cells/mL, and $1490 \cdot 10^6$ cells/mL for increasing IV doses at 168 h, and returned to baseline at 384 h. In addition, the baseline platelet counts were different between the dosing groups. All individual platelet counts for cynomolgus monkey were adequately described by the model. The estimate of the T_P parameter was 4.8 days and the estimate of T_{PLT} was 7.1 days. The S_{max} and RO_{thr} estimates were approximately 2-fold higher than for rhesus monkeys.

Model-Based Simulations

The ratio PLT_{max}/PLT_0 as a function of dose, stratified by route of administration, is shown in Fig. 5. The shape of the dose-response curve for rats is different from those for monkeys. The hyperbolic increase starts at lower doses (i.e. <0.01 mg/kg) and continues until reaching a plateau of 3.9. The dose-response curves are similar for rhesus and cynomolgus monkeys. They start to increase at higher doses than rats (i.e. 0.1–1 mg/kg) and increase without reaching a plateau in the simulated dose range. The maximal PLT_{max}/PLT_0 value predicted by the model was equivalent to the $1+S_{max}$, which was achieved for rats. The mean observed values of PLT_{max}/PLT_0 at the highest administered doses of 0.3, 5, and 5 mg/kg were 4.5, 2.4, and 2.7 for rats, rhesus monkeys, and cynomolgus monkeys, respectively. Similar trends were observed after SC romiplostim administration.

The relationships between the romiplostim serum concentration and the fractional receptor occupancy (RO) for the three species are graphically presented in Fig. 6. The RO was calculated as DR/R_{tot} from Eq. 6 and plotted against C. The curve for rats lies to the left of the curves for rhesus and cynomolgus monkeys, which are close to each other. Since the K_D value represents the romiplostim serum

Fig. 2 Romiplostim serum concentrations (upper panels) and platelet counts (lower panels) in rats following IV bolus (**a**) and SC (**b**) administration. Symbols represent the observed data. The solid line represents the median of the model predictions whereas the shaded region is limited by the 5th and 95th percentile of the simulated model predictions. Parameter estimates are shown in Table II.

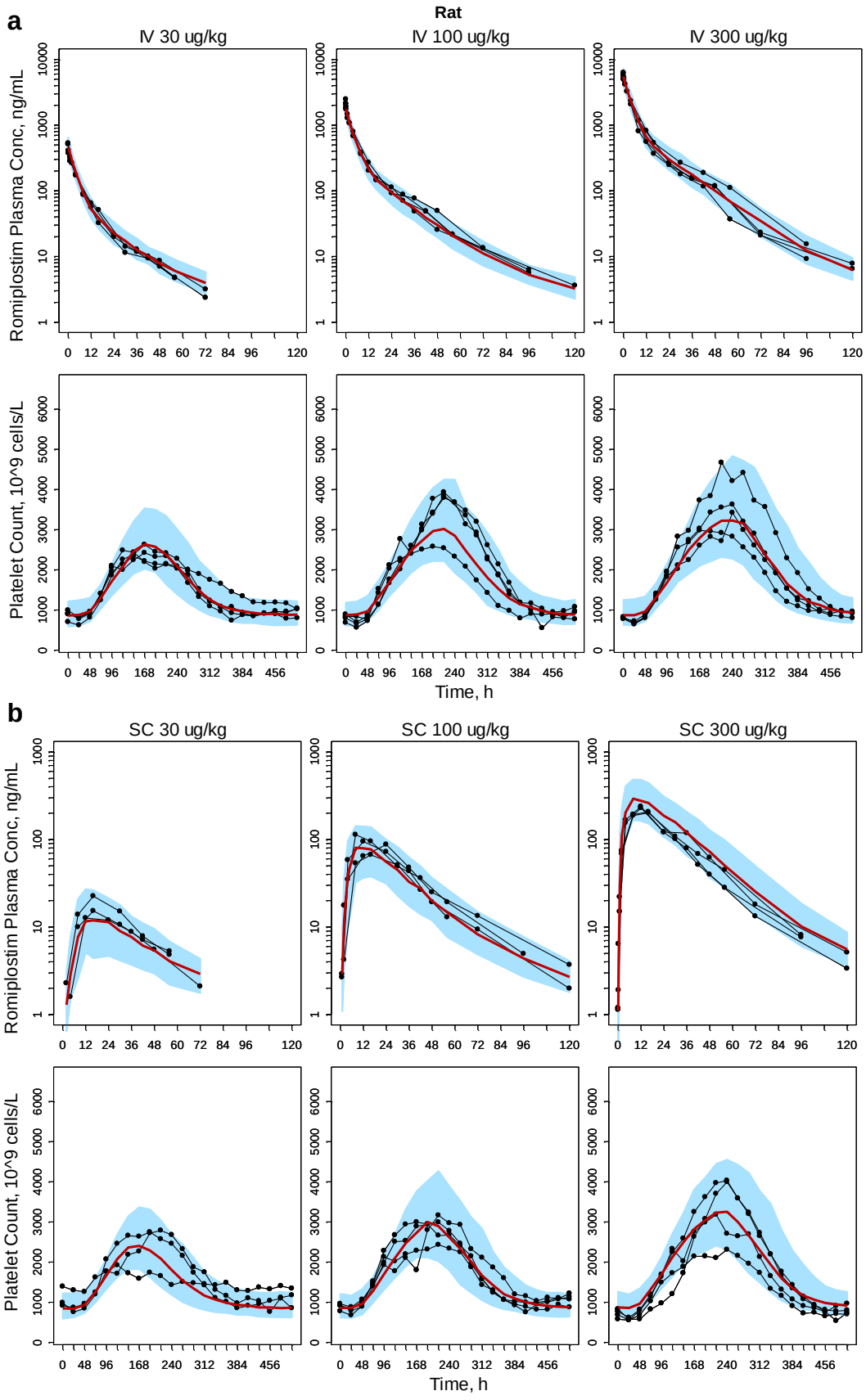
a
Rat
IV 30 ug/kg
IV 100 ug/kg
IV 300 ug/kg
Romiplostim Plasma Conc, ng/mL
Platelet Count, 10^9 cells/L
Time, h
b
SC 30 ug/kg
SC 100 ug/kg
SC 300 ug/kg
Romiplostim Plasma Conc, ng/mL
Platelet Count, 10^9 cells/L
Time, h

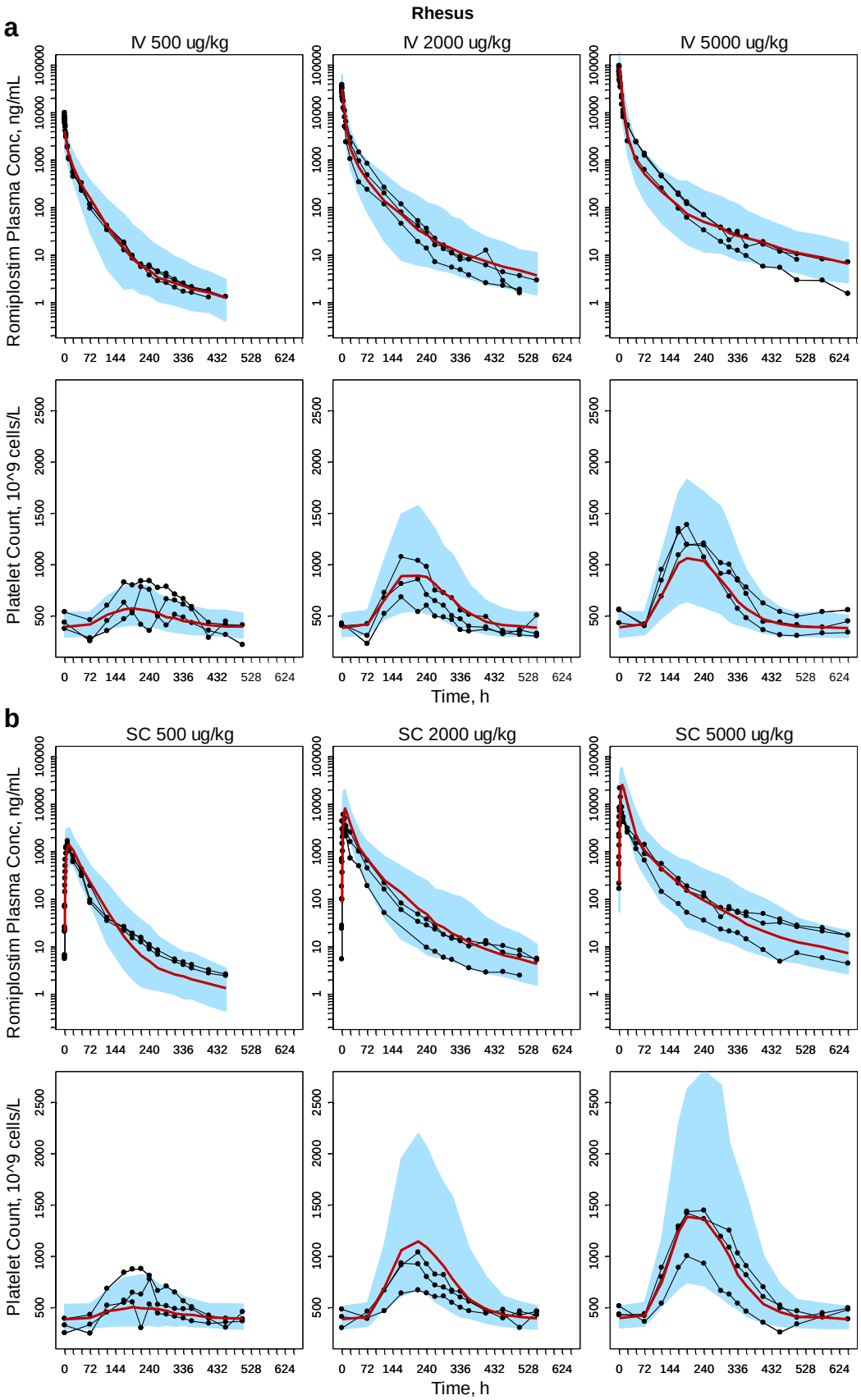
Rhesus
a
IV 500 ug/kg
IV 2000 ug/kg
IV 5000 ug/kg
Romiplostim Plasma Conc, ng/mL
Platelet Count, 10^9 cells/L
b
SC 500 ug/kg
SC 2000 ug/kg
SC 5000 ug/kg
Time, h

Fig. 3 Romiplostim serum concentrations (upper panels) and platelet counts (lower panels) in rhesus monkeys following IV bolus (**a**) and SC (**b**) administration. Symbols represent the observed data. The solid line represents the median of the model predictions whereas the shaded region is limited by the 5th and 95th percentile of the simulated model predictions. Parameter estimates are shown in Table II.

concentrations achieving 50% of receptor occupancy and the K_D ratios were 573 for rhesus monkeys to rats and 106 for cynomolgus monkeys to rats, the data indicate that romiplostim is by far more potent in rats than in monkeys, which is consistent with the dose-response relationships presented in Fig. 5. These relationships permit calculation of the romiplostim serum concentrations corresponding to the threshold of the fractional occupancy RO_{thr}. These were 1.638, 1452, and 1444 ng/mL for rats, rhesus, and cynomolgus monkeys, respectively.

DISCUSSION

Romiplostim target-mediated disposition was indicated by a dose-dependent decrease in V_{ss} based on the non-compartmental analysis. Since a significant fraction of the drug amount, relative to the dose, is bound to the receptors, and the pharmacological response to romiplostim, controlled by the drug receptor interaction, results in a dose-dependent increase in platelet counts and c-Mpl receptors, a simultaneous estimation of the PK and PD model parameters was performed by analyzing jointly PK and PD data in Sprague-Dawley rats, rhesus monkeys, and cynomolgus monkeys as previously suggested (19).

The estimates of the V were similar for all species (0.051–0.071 L/kg) and comparable to the blood volumes of 0.1 L/

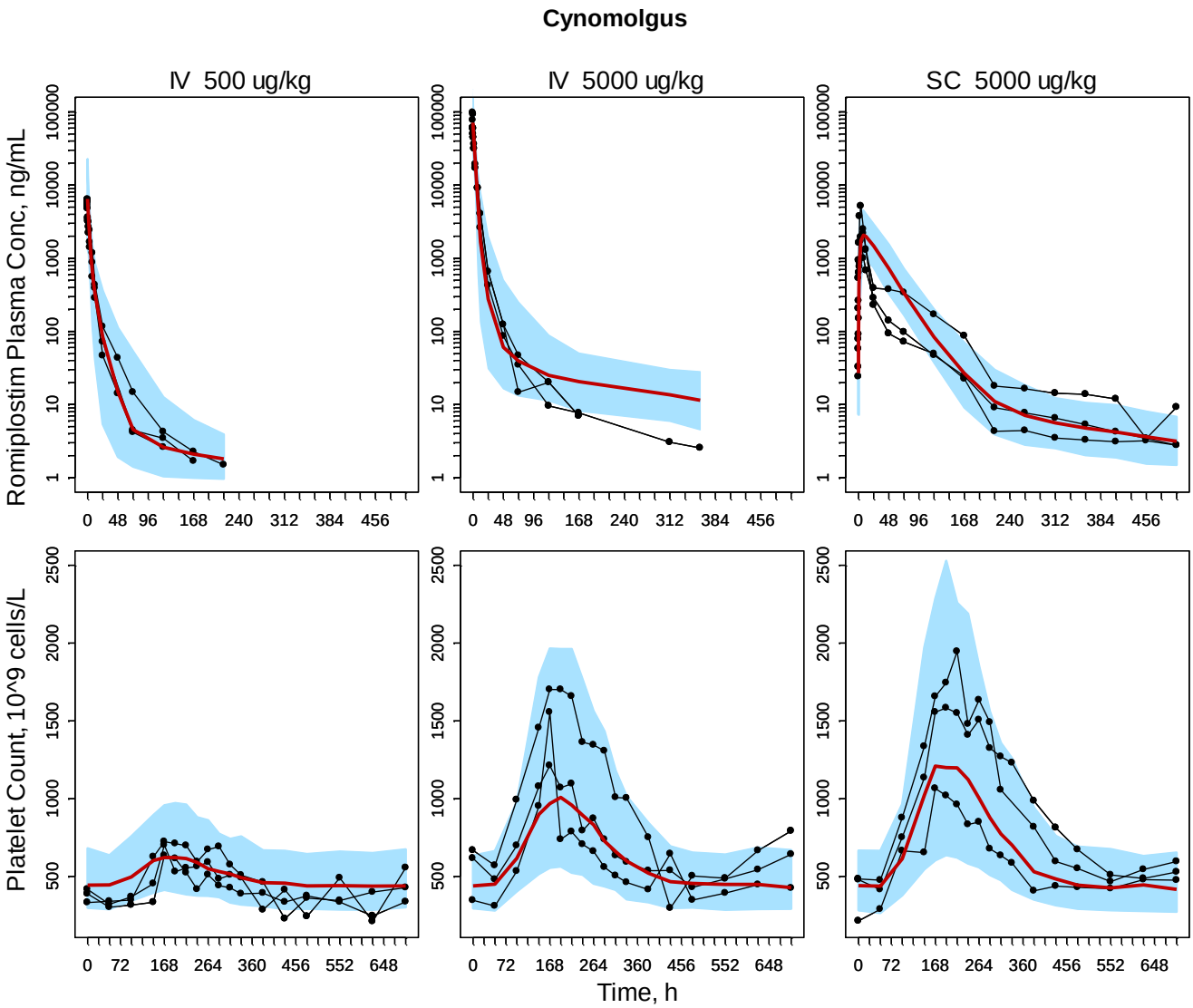

Fig. 4 Romiplostim serum concentrations (upper panels) and platelet counts (lower panels) in cynomolgus monkeys following IV bolus and SC administration. Symbols represent the observed data. The solid line represents the median of the model predictions whereas the shaded region is limited by the 5th and 95th percentile of the simulated model predictions. Parameter estimates are shown in Table II.

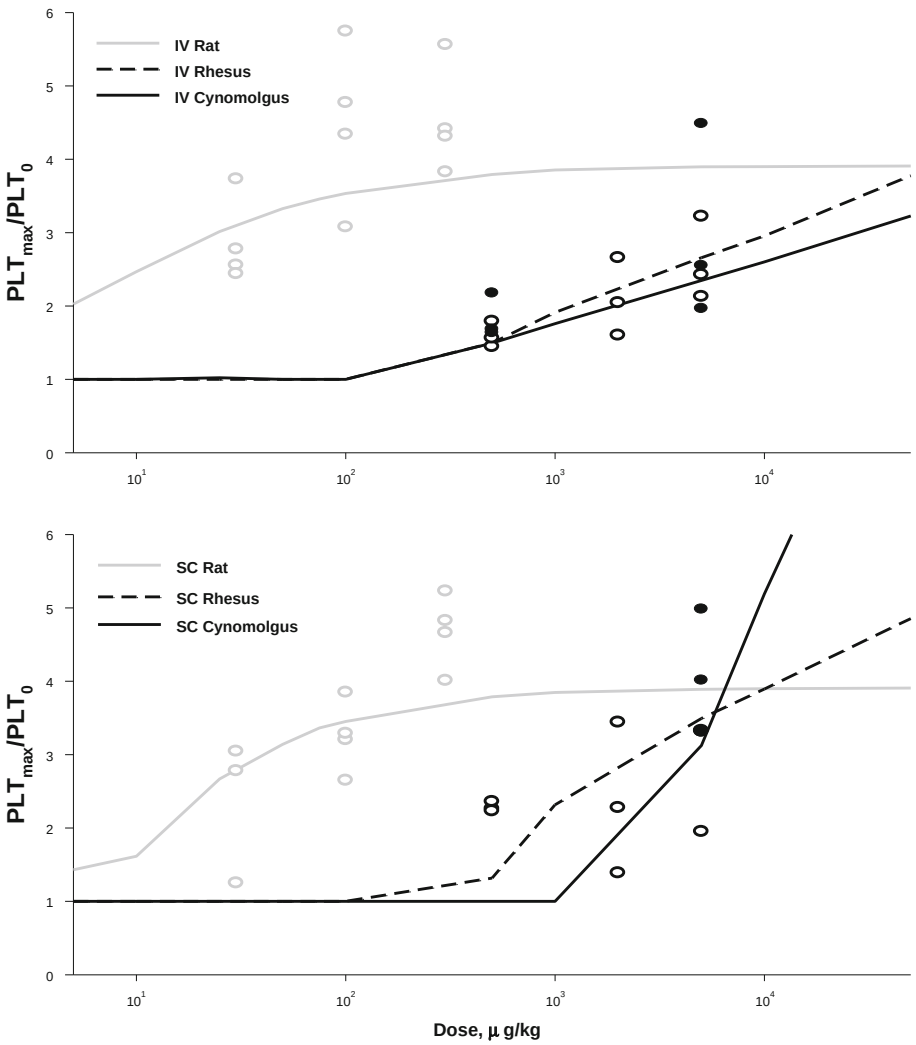

Fig. 5 Simulated (lines) romiplostim dose - response relationships for rats and monkeys by route of administration: IV bolus (upper panel) and SC dosing (lower panel). The symbols represent the observed data for individual animals: rat (gray open), rhesus (black open), cynomolgus (black solid). The parameter values used for simulations are the population estimates shown in Table II.

kg corrected by a hematocrit of 40% (33) and the estimates obtained in humans (19). The total CL for studied animals was similar and ranging 7.26 to 19.7 ml/h/kg. The linear elimination of romiplostim is due to the cellular uptake of the peptibody and binding to the FcRn receptor, as well as the elimination through the reticuloendothelial system. The Fc carrier domain of romiplostim contains the CH2 and CH3 regions of human immunoglobulin G subtype 1 (IgG1). IgG1 is a ligand for the FcRn receptor, which protects romiplostim from endosomal degradation and recycles it back to the circulation (34). As demonstrated in studies with FcRn knock-out and wild-type mice, romiplostim binds to the FcRn salvage receptor and undergoes endothelial recirculation, resulting in a substantially longer half-life than the TPO mimetic peptide alone (11). The parent molecule and clipped products undergo reticuloendothelial elimination, and smaller proteins are often filtered by the glomeruli and undergo tubular reabsorption and elimination (35). Therefore, the clearance mediated by FcRn is a major catabolic pathway for antibodies (36) and romiplostim, although the elimination rate is relatively slow.

The influence of FcRn on IgG tissue distribution has been studied by using physiologically-based PK models (37,38). In addition, a PK model of IgG disposition has been

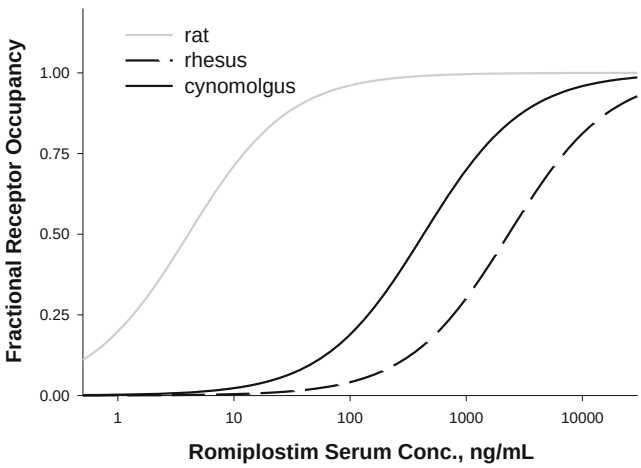

Fig. 6 Simulated fractional receptor occupancy as a function of romiplostim serum concentration for rats and monkeys. The receptor occupancy was calculated as $DR/R_{tot.}$ from Eq. 4.

previously developed, in which cellular uptake is represented by a first-order process, the fraction of bound drug is recycled to the plasma, and the free endosomal fraction is degraded at a first-order rate (39,40). In our analysis, a noticeable difference was observed between the estimates for the distributional clearances for rats and monkeys. Low values of these estimates for monkeys and their high coefficients of variation indicate a negligible impact of the distribution to a peripheral compartment on the romiplostim PK for applied doses. The volumes of the peripheral compartment were similar to the volumes of the central compartment for rats and rhesus monkeys. For the cynomolgus monkeys the former was 4.7 higher than the latter. This indicates a possibility of romiplostim tissue distribution and/or nonspecific binding. The peripheral volume of distribution for humans was larger than the V (19). Relative to humans, the absorption rate is 2.7-, 4.6-, and 1.5-fold faster for rats, rhesus, and cynomolgus monkeys, respectively, while the SC bioavailability was 39% lower, 100% higher, and 25% lower for rats, rhesus and cynomolgus monkeys, respectively, relative to humans.

The romiplostim to c-Mpl receptor binding model was developed using a minimal number of parameters to account for this process. A rapid binding assumption was implemented to avoid estimation of k_{on} and k_{off}, but estimates K_D as k_{off}/k_{on}. The estimate of rat K_D (68.6 pM) is close to the *in vitro* values reported for eTPO for both platelets (100–200 pM) and megakaryocytes (749 pM), and was also slightly higher than the *in vivo* recombinant human thrombopoietin (rHuTPO) K_D estimated using modeling techniques (45 pM) (3,17,41,42); however, it is much higher than the *in vitro* romiplostim K_D value determined for rats (4 pM) and the K_D estimate for romiplostim in healthy subjects (2.2 pM), which indicates that romiplostim has a high affinity for rat c-Mpl receptor. However, the estimate of K_D in rhesus and cynomolgus monkeys (39.3 and 7.27 nM, respectively) indicates that romiplostim has a lower affinity for monkey c-Mpl receptor and, consequently, is a more potent drug in rats than in monkeys by an order of 100. In that regard, the romiplostim pharmacokinetics and pharmacodynamics in rat is more similar to human than that observed in monkeys.

The proposed model extends the previously model for romiplostim in humans by introducing more mechanistically sound processes (19). Since the general TMDD model also includes receptor turnover (14), the previous assumption that the number of total receptors was proportional to the platelet counts has been extended to the number of platelets and megakaryocytes. This implies that c-Mpl receptor turnover is no longer solely driven by platelet lifespan. Rather, it is estimated based on T_p and T_{PLT} across the species analyzed, although the precision of these estimates is not optimal given the lack of direct c-Mpl measurements. The calculated values of the baseline total c-Mpl receptors based on Eq. 5 were 1.33 nM, 136 nM and 16.6 nM for rat, rhesus and cynomolgus monkey, respectively. The analogous value for humans calculated from Eq. 1 in (19) was 0.91 nM.

Similar to other TPO-stimulating agents, the estimated value of k_{int} was negligible (18) as expected from the romiplostim molecular weight, which could prevent the internalization mediated by c-Mpl. However, it implies that a romiplostim clearance pathway related to elimination of platelets from the circulation was ignored. This hypothesis should be cautiously interpreted because of the lack of information about the internalization process. It could be just an artifact due to the lack of information on the data with respect to the binding process. In fact, the sensitivity analysis performed on a general quasi-equilibrium approximation of TMDD model indicates that the drug concentration profiles below the K_D value provide the most information about k_{int} (43). These points were hardly present in the analyzed rat data, although they are available from monkeys.

The estimates of T_{PLT} ranged from 6.2 to 7.6 days and were close to the reported values of 5 days for rat and 6.5 days for monkey (44,45). The estimated values of T_P were determined by the lag time in the platelet responses, which implies that T_P reflects the time required for precursor cells to mature before they release platelets into the circulation. The delay in the time to peak platelet response and a prolonged duration of the PD effect with increasing romiplostim dose can be attributed to nonlinearity in PK, because in the current model, the romiplostim stimulatory effect is driven by receptor occupancy rather than the romiplostim serum concentration. The PK nonlinearity resulted from saturation of the receptor occupancy, which leads to a longer maximal stimulation of platelet production. Its impact on PD is an increase in the time to achieve maximum platelet counts and to return to baseline values across the species analyzed.

Consequently, the differences in the K_D estimates across species are reflected in the dose-response relationships for all three species, in which a 100-fold difference between rats and monkeys was required to elicit a 2-fold increase in platelet counts. All species exhibit an on-and-off stimulatory effect with the threshold receptor occupancy determined by the RO_{thr} parameter that was estimated in the range 39–77% for monkeys, which implies that a relatively large percentage of c-Mpl receptors need to be occupied to produce the PD effect. However, in rats, only 29% of c-Mpl receptors need to be occupied to produce the PD effect. This suggests an indirect relationship between binding to the c-Mpl receptor and drug effect (41), consistent with the spare receptor theory (46) and the biochemical cascade in receptor signaling (4). Previously, we estimated that a receptor occupancy of 28% is required to achieve 50% of the maximal stimulatory effect of romiplostim in healthy subjects. These values were similar to the value previously

reported by Samtani *et al.* with data from another compound, and differ substantially from the value estimated for rhesus monkeys. The maximal stimulus in monkeys ranges from 9.3 to 18.9, which is similar to the previously estimated value in healthy subjects, 11.2 (19).

Taken together, these results confirm the high potency of romiplostim and explain why platelet responses were similar after IV and SC administration at the same dose levels, despite the large differences in the PK exposures across the species. The limited number of TPO receptors can be readily saturated with the relatively high concentrations achieved after IV administration of romiplostim, which may lead to considerable dose wastage and a reduction of drug efficiency relative to the SC route, in which the prolonged absorption provides relatively lower serum concentrations leading to reduced receptor saturation but longer-lasting effects than after IV administration. This increase in drug efficiency may also compensate for the incomplete SC bioavailability observed in rat and cynomolgus monkey.

In summary, the established PDMDD model adequately described romiplostim serum concentrations and platelet counts in rats, rhesus monkeys, and cynomolgus monkeys following IV bolus and SC administration. The model quantified the contribution of linear clearance and c-Mpl receptor-mediated binding to the disposition of romiplostim. Romiplostim is much more potent in rats than in rhesus and cynomolgus monkeys. The model served to simulate dose-response relationships in the animals studied.

ACKNOWLEDGMENTS

This study was supported by an educational donation for the Fellowship in PK/PD Hematology from Amgen Inc. The authors wish to thank Teresa Wong for the bioanalytical support, Michelle Zakson for editing/writing assistance.

This study was funded by Amgen Inc. L Sutjandra, JJ Perez-Ruixo, B Sloey, AT Chow, and YM Wang were employees at Amgen, Inc. at the time this analysis was performed. W Krzyzanski was a consultant for Amgen, Inc, and received consultation fees for this project.

Part of the content of this manuscript was presented at a poster podium session: Y. Wang, W. Krzyzanski, J. Xiao, B. Jaramilla, A. Chow, Pharmacokinetic and Pharmacodynamic modeling of AMG 531, a thrombopoiesis stimulating Fc fusion protein (peptibody), in rats and monkeys. The AAPS Journal Vol. 9, No. S2, Abstract W4407 (2007).

REFERENCES

1. Methia N, Louache F, Vainchenker W, Wendling F. Oligodeoxynucleotides antisense to the proto-oncogene c-mpl specifically inhibit *in vitro* megakaryocytopoiesis. Blood. 1993;82:1395–401.
2. Sheridan WP, Choi E, Toombs CF, Nichol J, Fanucchi M, Basser RI. Biology of thrombopoiesis and the role of Mpl ligand in the production and function of platelets. Platelets. 1997;8:319–32.
3. Broudyand VC, Lin NL. AMG531 stimulates megakaryopoiesis *in vitro* by binding to Mpl. Cytokine. 2004;25:52–60.
4. Geddis AE, Linden HM, Kaushansky K. Thrombopoietin: a pan-hematopoietic cytokine. Cytokine Growth Factor Rev. 2002; 13:61–73.
5. Basser RL, O'Flaherty E, Green M, Edmonds M, Nichol J, Menchaca DM, Cohen B, Begley CG. Development of pancytopenia with neutralizing antibodies to thrombopoietin after multicycle chemotherapy supported by megakaryocyte growth and development factor. Blood. 2002;99:2599–602.
6. Li J, Yang C, Xia Y, Bertino A, Glaspy J, Roberts M, Kuter DJ. Thrombocytopenia caused by the development of antibodies to thrombopoietin. Blood. 2001;98:3241–8.
7. Wang B, Nichol JL, Sullivan JT. Pharmacodynamics and pharmacokinetics of AMG 531, a novel thrombopoietin receptor ligand. Clin Pharmacol Ther. 2004;76:628–38.
8. Molineuxand G, Newland A. Development of romiplostim for the treatment of patients with chronic immune thrombocytopenia: from bench to bedside. Br J Haematol. 2010;150:9–20.
9. Bussel JB, Kuter DJ, George JN, McMillan R, Aledort LM, Conklin GT, Lichtin AE, Lyons RM, Nieva J, Wasser JS, Wiznitzer I, Kelly R, Chen CF, Nichol JL. AMG 531, a thrombopoiesis-stimulating protein, for chronic ITP. N Engl J Med. 2006;355:1672–81.
10. Li J, Xia Y, Kuter DJ. Interaction of thrombopoietin with the platelet c-mpl receptor in plasma: binding, internalization, stability and pharmacokinetics. Br J Haematol. 1999;106:345–56.
11. Wang YM, Sloey B, Wong T, Khandelwal P, Melara R, Sun YN. Investigation of the Pharmacokinetics of romiplostim in rodents with a focus on the clearance mechanism. Pharm Res. 2011;28:1931–38.
12. Levy G. Pharmacologic target-mediated drug disposition. Clin Pharmacol Ther. 1994;56:248–52.
13. Sugiyamaand Y, Hanano M. Receptor-mediated transport of peptide hormones and its importance in the overall hormone disposition in the body. Pharm Res. 1989;6:192–202.
14. Mager and DE, Jusko WJ. General pharmacokinetic model for drugs exhibiting target-mediated drug disposition. J Pharmacokinet Pharmacodyn. 2001;28:507–32.
15. Woo S, Krzyzanski W, Jusko WJ. Target-mediated pharmacokinetic and pharmacodynamic model of recombinant human erythropoietin (rHuEPO). J Pharmacokinet Pharmacodyn. 2007;34:849–68.
16. Roskos LK, Lum P, Lockbaum P, Schwab G, Yang BB. Pharmacokinetic/pharmacodynamic modeling of pegfilgrastim in healthy subjects. J Clin Pharmacol. 2006;46:747–57.
17. Jinand F, Krzyzanski W. Pharmacokinetic model of target-mediated disposition of thrombopoietin. AAPS PharmSci. 2004;6:E9.
18. Samtani MN, Perez-Ruixo JJ, Brown KH, Cerneus D, Molloy CJ. Pharmacokinetic and pharmacodynamic modeling of pegylated thrombopoietin mimetic peptide (PEG-TPOm) after single intravenous dose administration in healthy subjects. J Clin Pharmacol. 2009;49:336–50.
19. Wang YM, Krzyzanski W, Doshi S, Xiao JJ, Perez-Ruixo JJ, Chow AT. Pharmacodynamics-mediated drug disposition (PDMDD) and precursor pool lifespan model for single dose of romiplostim in healthy subjects. AAPS J. 2010;12:729–40.
20. Hayashi N, Tsukamoto Y, Sallas WM, Lowe PJ. A mechanism-based binding model for the population pharmacokinetics and pharmacodynamics of omalizumab. Br J Clin Pharmacol. 2007;63:548–61.
21. Ng CM, Stefanich E, Anand BS, Fielder PJ, Vaickus L. Pharmacokinetics/pharmacodynamics of nondepleting anti-CD4

monoclonal antibody (TRX1) in healthy human volunteers. Pharm Res. 2006;23:95–103.
22. Sutjandra L, Rodriguez RD, Doshi S, Ma M, Peterson MC, Jang GR, Chow AT, Pérez-Ruixo JJ. Population pharmacokinetic meta-analysis of denosumab in healthy subjects and postmenopausal women with osteopenia or osteoporosis. Clin Pharmacokinet. 2011;50:793–807.
23. Mager DE, Neuteboom B, Efthymiopoulos C, Munafo A, Jusko WJ. Receptor-mediated pharmacokinetics and pharmacodynamics of interferon-beta1a in monkeys. J Pharmacol Exp Ther. 2003;306: 262–70.
24. Segrave AM, Mager DE, Charman SA, Edwards GA, Porter CJ. Pharmacokinetics of recombinant human leukemia inhibitory factor in sheep. J Pharmacol Exp Ther. 2004;309:1085–92.
25. Magerand DE, Krzyzanski W. Quasi-equilibrium pharmacokinetic model for drugs exhibiting target-mediated drug disposition. Pharm Res. 2005;22:1589–96.
26. Harker LA, Roskos LK, Marzec UM, Carter RA, Cherry JK, Sundell B, Cheung EN, Terry D, Sheridan W. Effects of megakaryocyte growth and development factor on platelet production, platelet life span, and platelet function in healthy human volunteers. Blood. 2000;95:2514–22.
27. Perez-Ruixo JJ, Krzyzanski W, Hing J. Pharmacodynamic analysis of recombinant human erythropoietin effect on reticulocyte production rate and age distribution in healthy subjects. Clin Pharmacokinet. 2008;47:399–415.
28. Krzyzanski W. Interpretation of transit compartments pharmacodynamic models as lifespan based indirect response models. J Pharmacokinet Pharmacodyn. 2011;38:179–204.
29. Bauer R. NONMEM Users Guide Introduction to NONMEM 7.2.0, ICON Development Solutions Ellicott City, MD, 2011.
30. Yano Y, Beal S, Sheiner LB. Evaluating pharmacokinetic/pharmacodynamic models using the posterior predictive check. J Pharmacokinet Pharmacodyn. 2001;28:171–92.
31. Yang C, Li YC, Kuter DJ. The physiological response of thrombopoietin (c-Mpl ligand) to thrombocytopenia in the rat. Br J Haematol. 1999;105:478–85.
32. Krzyzanski W, Perez Ruixo JJ. Lifespan based indirect response models. J Pharmacokinet Pharmacodyn. 2012;39:109–23.
33. Schremer S. The blood morphology of laboratory animals. Philadelphia: F. A. Davis Company; 1967.
34. Lobo ED, Hansen RJ, Balthasar JP. Antibody pharmacokinetics and pharmacodynamics. J Pharm Sci. 2004;93:2645–68.
35. Israel EJ, Wilsker DF, Hayes KC, Schoenfeld D, Simister NE. Increased clearance of IgG in mice that lack beta 2-microglobulin: possible protective role of FcRn. Immunology. 1996;89:573–8.
36. Waldmannand TA, Strober W. Metabolism of immunoglobulins. Prog Allergy. 1969;13:1–110.
37. Ferl GZ, Wu AM, DiStefano 3rd JJ. A predictive model of therapeutic monoclonal antibody dynamics and regulation by the neonatal Fc receptor (FcRn). Ann Biomed Eng. 2005;33:1640–52.
38. Gargand A, Balthasar JP. Physiologically-based pharmacokinetic (PBPK) model to predict IgG tissue kinetics in wild-type and FcRn-knockout mice. J Pharmacokinet Pharmacodyn. 2007;34: 687–709.
39. Xiao JJ, Krzyzanski W, Wang YM, Li H, Rose MJ, Ma M, Wu Y, Hinkle B, Perez-Ruixo JJ. Pharmacokinetics of anti-hepcidin monoclonal antibody Ab 12B9m and hepcidin in cynomolgus monkeys. AAPS J. 2010 12(4):646–57.
40. Hansen and RJ, Balthasar JP. Pharmacokinetic/pharmacodynamic modeling of the effects of intravenous immunoglobulin on the disposition of antiplatelet antibodies in a rat model of immune thrombocytopenia. J Pharm Sci. 2003;92:1206–15.
41. Kuterand DJ, Begley CG. Recombinant human thrombopoietin: basic biology and evaluation of clinical studies. Blood. 2002;100:3457–69.
42. Sato T, Fuse A, Niimi H, Fielder PJ, Avraham H. Binding and regulation of thrombopoietin to human megakaryocytes. Br J Haematol. 1998;100:704–11.
43. Abraham AK, Krzyzanski W, Mager DE. Partial derivative-based sensitivity analysis of models describing target-mediated drug disposition. AAPS J. 2007;9:E181–9.
44. Corash L, Shafer B, Perlow M. Heterogeneity of human whole blood platelet subpopulations. II. Use of a subhuman primate model to analyze the relationship between density and platelet age. Blood. 1978;52:726–34.
45. Hjortand PF, Paputchis H. Platelet life span in normal, splenectomized and hypersplenic rats. Blood. 1960;15:45–51.
46. Stephenson RP. A modification of receptor theory. Br J Pharmacol Chemother. 1956;11:379–93.